CHEMISTRY
A EUROPEAN JOURNAL

DOI: 10.1002/chem.200800723

Magnetic Structure and Electronic Study of Complex Oxygen-Deficient Manganites

Raquel Cortés-Gil,[a, b] María Hernando,[a] M. Luisa Ruiz-González,[a] Eva Céspedes,[c] Carlos Prieto,[c] José M. Alonso,[b, c] María Vallet-Regí,[b, d] Antonio Hernando,[b, e] and José M. González-Calbet*[a, b]

Abstract: Neutron diffraction and X-ray absorption near-edge structure (XANES) studies have been performed in $La_{0.5}Ca_{0.5}MnO_{2.5}$, $La_{0.5}Sr_{0.5}MnO_{2.5}$ and $Nd_{0.5}Sr_{0.5}MnO_{2.5}$ oxygen-deficient perovskite compounds obtained by topotactic reduction. They all exhibit a brownmillerite structure with G-type antiferromagnetic ordering. Mn^{2+}, Mn^{3+} and Mn^{4+} coexist at the octahedral sites, whereas only Mn^{2+} is placed in the tetrahedral positions. A magnetic moment of 1.6 μ_B has been detected at the tetrahedral layers, which can be explained by assuming Mn^{2+} is in a low-spin configuration.

Keywords: magnetic properties · manganese · neutron diffraction · perovskite phases · X-ray absorption spectroscopy

Introduction

Tunability of oxygen non-stoichiometry is a common strategy in ABO_3 perovskite-related systems to deal with new phases and interesting associated properties, as a consequence of structural and charge balance accommodation. The route to stabilize new superstructures is not evident, the chemical nature of the sample being crucial as well as the strict control of the synthesis conditions.[1,2] In some cases, even if the number of oxygen vacancies is relatively high, the system develops disordered patterns of non-occupied oxygen positions instead of ordered ones. Under different circumstances, the adequate combination of cations in either the A or B sub-lattices leads to homologous series of ordered superstructures. This is the case for the $A_nB_nO_{3n-1}$ family,[3] where $n-1$ octahedral layers inter-grow with a tetrahedral one. This homologous series involves a systematic pathway through which perovskite compounds can accommodate oxygen vacancies as a consequence of their ordered arrangement, which leads to the formation of tetrahedra. The $n=2$ term can be described from the alternation of one octahedral layer ($n-1$) and a tetrahedral one. This description corresponds to the brownmillerite structure,[4] in agreement with the $A_2B_2O_5$ general composition. Three symmetry space groups, *Ibm*2, *Pnma* and *Icmm*, have been described for brownmillerite compounds depending on the equatorial oxygen arrangement.[5–7]

Further to this structural description, oxygen engineering is a proved important tool for on-demand tailoring of perovskite-related compounds into optimized performances. In this sense, the control of oxygen content has played a paramount role on the properties of different HTSC perovskite-related families.[8] Moreover, in the last few years, a lot of research has been devoted to manganese-related perovskites, $La_{1-x}A_xMnO_3$, as a consequence of their intriguing magnetic and electric behaviour mainly related to Mn^{3+} and Mn^{4+} coexistence. Although much of the study has been focused on the compositional variations at the A position of

[a] Dr. R. Cortés-Gil, Dr. M. Hernando, Dr. M. L. Ruiz-González, Prof. J. M. González-Calbet
Dpto. Química Inorgánica
Facultad de Químicas
Universidad Complutense de Madrid, 28040 Madrid (Spain)
Fax: (+34) 91-3944342
E-mail: jgcalbet@quim.ucm.es

[b] Dr. R. Cortés-Gil, Dr. J. M. Alonso, Prof. M. Vallet-Regí, Prof. A. Hernando, Prof. J. M. González-Calbet
Instituto de Magnetismo Aplicado, UCM-CSIC-ADIF
Las Rozas, P.O. Box 155, 28230 Madrid (Spain)

[c] E. Céspedes, Dr. C. Prieto, Dr. J. M. Alonso
Instituto de Ciencia de Materiales, CSIC
Sor Juana Inés de la Cruz s/n, 28049 Madrid (Spain)

[d] Prof. M. Vallet-Regí
Dpto. Química Inorgánica y Bioinorgánica
Facultad de Químicas, Universidad Complutense de Madrid
28040 Madrid (Spain)

[e] Prof. A. Hernando
Dpto. Física de Materiales, Facultad de Físicas
Universidad Complutense de Madrid, 28040-Madrid (Spain)

the perovskite sub-lattice, just recently there has been some effort to extend it to the oxygen sub-lattice. For instance, the remarkable stabilization of several Mn-related brownmillerites as Sr_2MnGaO_5[9] and $SrCaMnGaO_5$,[10] which are considered useful as cathodes for solid oxide fuel cell (SOFC) applications, has been reported. Notice, however, that in all cases the compounds respond to the general formula A_2MnBO_5 with a B^{3+} cation needed for the stabilization of the brownmillerite phase. This cation is non-magnetic and occupies the tetrahedral positions, whereas Mn is at the octahedral ones. They all exhibit 3D magnetic interactions and G-type antiferromagnetic (AFM) structure with the magnetic moments of Mn atoms antiparallel either in the octahedral layers or in between them.[11] Analogous phases with only Mn at the B position are quite difficult to stabilize. However, under strict oxygen control, it is possible to stabilize ordered $La_{1-x}A_xMnO_{3-\delta}$ oxygen-deficient phases by topotactic reduction of the parent perovskite. Following this procedure, we have obtained the $La_{0.5}Ca_{0.5}MnO_{2.5}$,[12] $La_{0.5}Sr_{0.5}MnO_{2.5}$[13] and $Nd_{0.5}Sr_{0.5}MnO_{2.5}$[14] brownmillerite compounds as well as the $La_4Mn_4O_{11}$[15] $n=4$ term of the $A_nB_nO_{3n-1}$ homologous series.

Casey et al.[16] reported new brownmillerite-related materials in the $La_{1-x}Sr_xMnO_{2.5}$ ($0.2 \le x \le 0.4$) system. Neutron and electron diffraction data for $x=0.2$ and 0.25 materials show $P2_1/c$ monoclinic structures with ordered alternation of twisted chains of Mn(II) tetrahedra, whereas for the $x=0.4$ composition the twisted chains of tetrahedra are disordered in an orthorhombic material. No magnetic characterization of these phases is reported. Returning to the $La_{0.5}Ca_{0.5}MnO_{2.5}$, $La_{0.5}Sr_{0.5}MnO_{2.5}$ and $Nd_{0.5}Sr_{0.5}MnO_{2.5}$ phases, it is worth mentioning the different magnetic behaviour corresponding to the isostructural brownmillerite phases. Although all of them exhibit AFM ordering with Neel temperature (T_N) around 150 K, $La_{0.5}Sr_{0.5}MnO_{2.5}$ also exhibits ferromagnetic (FM) interactions.[13,14] This behaviour resembles that observed on the full oxidized precursor perovskites and it seems to remain in the topotactic reducing processes. The existence of FM interactions in the $La_{0.5}Sr_{0.5}MnO_3$ perovskite is related to double exchange interactions through Mn^{3+}-O-Mn^{4+} angles of 180°. The increase of the orthorhombic distortion, which leads to smaller Mn-O-Mn angles, in the Nd/Sr and La/Ca perovskites justifies the gradual disappearance of such FM behaviour.[17] Therefore, a careful neutron diffraction (ND) study has been performed in the corresponding reduced compounds to gather both crystallographic and magnetic structure information.

Furthermore, the magnetic and electric properties of these systems strongly depend on the Mn oxidation state. Actually, the FM interactions in Mn perovskites usually require both Mn^{3+} and Mn^{4+}. The reduction process is necessarily accompanied by changes in the oxidation states, and it is logical to think about 50% Mn^{3+} and 50% Mn^{2+} for 2.5 oxygen content. However, low-energy X-ray absorption spectroscopy (XAS) studies performed at the Mn L-edge in $La_{0.5}Ca_{0.5}MnO_{2.5}$[18] indicate a more complex situation due to the coexistence of three oxidation states: Mn^{2+}, Mn^{3+} and Mn^{4+}. Actually, this brownmillerite-related material is obtained through a topotactic reduction process of $La_{0.5}Ca_{0.5}MnO_3$ which is also reversible. Reduction of $La_{0.5}Ca_{0.5}MnO_3$ and oxidation of $La_{0.5}Ca_{0.5}MnO_{2.5}$ can lead to $La_{0.5}Ca_{0.5}MnO_{3-\delta}$ samples with identical δ value but different magnetic and electric behaviour. Obviously, different properties shown by samples with identical δ value obtained as a function of the synthetic pathway can only be explained on the basis of three different Mn oxidation states, as confirmed by XAS characterization. This surprising behaviour modifies the landscape of the expected magnetic interactions. For this reason, an additional X-ray absorption near-edge structure (XANES) study at the high-energy Mn K-edge is also reported here for $La_{0.5}Sr_{0.5}MnO_{2.5}$.

Results and Discussion

Preliminary studies by means of X-ray and electron diffraction show the presence of I-centred brownmillerite with space group *Ibm*2 for the three compounds.[12–14] From these results, the crystal structures of $La_{0.5}Sr_{0.5}MnO_{2.5}$ and $Nd_{0.5}Sr_{0.5}MnO_{2.5}$ have been refined from ND data using the space group *Ibm*2 as starting model. *Pnma* and *Icmm* space groups were also considered but the best results were gathered for *Ibm*2. Actually, brownmillerite compounds, generally, crystallize in one of the two *Ibm*2[5] and *Pnma*[6] space groups. In some cases, a better fit of the Rietveld refinement is attained by using the *Icmm* space group[6,7,19,20] as a consequence of order–disorder phenomena involving the tetrahedral layers. This disorder is reflected as diffuse streaking on the selected-area electron diffraction (SAED) patterns along certain directions.[7,8] In the *Icmm* group, the 8*i* sites, which correspond to the metal lying at the tetrahedral position and on one of the oxygen atoms (O3), have mean occupancies of one half, thus allowing disordered displacements of these atoms. In fact, this situation could be also understood on the basis of disorder configurations of the tetrahedral layers in both *Ibm*2 and *Pnma* space groups, characteristic of the brownmillerite structure. SAED of the samples studied here did not show diffuse streaking.[13]

At room temperature, the samples are paramagnetic and exhibit orthorhombic structure with the *Ibm*2 space group proposed above. The Rietveld refinement patterns and difference plots for $La_{0.5}Sr_{0.5}MnO_{2.5}$ and $Nd_{0.5}Sr_{0.5}MnO_{2.5}$ are shown in Figure 1a and b, respectively. The final structural parameters resulting from these refinements are gathered in Table 1, and the corresponding interatomic selected distances (Mn–O) are collected in Table 2.

The resulting structure is depicted in Figure 2a and a schematic representation of the octahedral and tetrahedral environment is shown in Figure 2b. The Mn_2O_4 tetrahedra show three short, similar Mn–O distances and a longer one. The MnO_6 octahedra are quite elongated, which suggests a Jahn–Teller effect, with four short equatorial and two long apical distances. The distortion of the MnO_6 octahedra is an

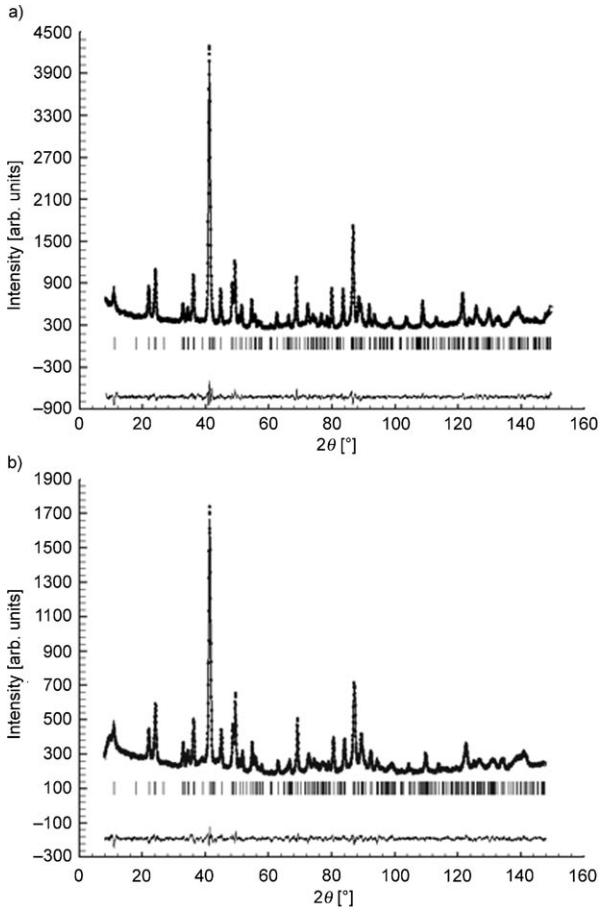

Figure 1. Observed, calculated and difference ND patterns corresponding to a) $La_{0.5}Sr_{0.5}MnO_{2.5}$ and b) $Nd_{0.5}Sr_{0.5}MnO_{2.5}$ at room temperature.

Table 1. Final structural parameters corresponding to $La_{0.5}Sr_{0.5}MnO_{2.5}$ and $Nd_{0.5}Sr_{0.5}MnO_{2.5}$.[a]

	$La_{0.5}Sr_{0.5}MnO_{2.5}$		$Nd_{0.5}Sr_{0.5}MnO_{2.5}$	
T [K]	300	5	300	5
Mn1 (0,0,0)				
B [Å^2]	1.36(9)	0.93(15)	1.9(1)	1.47(15)
M [μ_B]		2.64(6)		2.61(5)
Mn2 (x,$^1/_4$,z)				
x	−0.4591(18)	−0.45(2)	−0.4549(19)	0.452(2)
z	0.449(3)	−0.460(5)	0.457(4)	0.449(6)
B [Å^2]	0.4(1)	0.5(2)	2.06(18)	1.3(2)
M [μ_B]		1.63(7)		1.65(3)
Ln/Sr (x,y,z)				
x	0.5121(8)	0.5064(18)	0.4981(12)	0.4983(19)
y	0.6115(1)	0.61107(15)	0.61193(1)	0.61192(13)
z	0.008(3)	0.013(5)	0.007(5)	−0.004(4)
B [Å^2]	1.79(4)	1.27(6)	1.67(3)	1.50(6)
O1 (x,y,z)				
x	0.252(2)	0.246(4)	0.245(4)	0.247(3)
y	0.0017(6)	0.0017(11)	−0.0004(19)	0.0025(16)
z	0.263(3)	0.266(5)	0.255(5)	0.249(6)
B [Å^2]	1.23(4)	1.07(7)	1.68(5)	1.35(8)
O2 (x,y,z)				
x	0.008(1)	0.012(2)	0.0059(18)	0.004(2)
y	0.13639(14)	0.136(2)	0.13560(16)	0.1354(2)
z	0.011(3)	0.014(5)	−0.0004(19)	−0.017(5)
B11	0.037(2)	0.037(3)	0.0292(15)	0.0198(13)
B22	0.00154(7)	0.0010(1)	0.0018(7)	0.00158(8)
B33	0.0145(17)	0.014(2)	0.0229(14)	0.0256(15)
B12	0.00008(7)	0.002(1)	−0.0012(7)	−0.001(7)
O3 (x,$^1/_4$,z)				
x	0.557(3)	0.537(5)	0.5505(15)	0.553(2)
z	0.083(5)	0.093(3)	0.062(5)	0.055(6)
B11	0.076(9)	0.084(14)	0.033(4)	0.073(7)
B22	0.00159(19)	0.010(2)	0.00202(17)	0.0017(19)
B33	0.065(8)	0.046(8)	0.046(5)	0.038(6)
a [Å]	5.41059(15)	5.39548(17)	5.39311(13)	5.35052(14)
b [Å]	16.7525(3)	16.71952(4)	16.6253(4)	16.59203(3)
c [Å]	5.39599(14)	5.38090(17)	5.36388(12)	5.38066(14)

[a] Space group *Ibm*2. Fit parameters for: $La_{0.5}Sr_{0.5}MnO_{2.5}$: 300 K: R_F = 3.59, R_{exp} = 4.87, R_B = 4.04, χ^2 = 1.1; 5 K: R_F = 3.31, R_{exp} = 5.30, R_B = 5.52, χ^2 = 2.58, R_{mag} = 6.87; $Nd_{0.5}Sr_{0.5}MnO_{2.5}$: 300 K: R_F = 2.5, R_{exp} = 1.97, R_B = 5.52, χ^2 = 2.59; 5 K: R_F = 2.71, R_{exp} = 2.05, R_B = 6.12, χ^2 = 2.98, R_{mag} = 10.8.

important feature of the brownmillerite structure, which is observed, for instance, in $Sr_2Fe_2O_5$,[21] Sr_2MnGaO_5[9] or $Sr_2Co_{2-x}Ga_xO_5$.[19]

It is noteworthy that ND data are particularly useful in elucidating the distribution of oxygen atoms. In this sense, anisotropic thermal parameters for O1 and O2 atoms have been refined from the ND data for $Ln_{0.5}Sr_{0.5}MnO_{2.5}$ (Ln = La, Nd) compounds; the ellipsoids are shown in Figure 2a. These anisotropic thermal factors reveal the local disorder, which indicates significant delocalization of these atoms around the mean position. Such behaviour has also been observed in other brownmillerite-related structures, such as $Ba_2In_2O_5$ and $Sr_2Co_{2-x}Ga_xO_5$.[19,20]

Bond valence sum (BVS) calculations were performed by using bond lengths from Table 2 for $Ln_{0.5}Sr_{0.5}MnO_{2.5}$ (Ln = La, Nd) obtained from ND data refinement to establish any site preference, octahedral or tetrahedral, for the different oxidation states of Mn. The result is shown in Table 3 and demonstrates that the tetrahedral sites (Mn2) are occupied by Mn^{2+}, whereas an average oxidation state of Mn^{3+} is obtained in the octahedral site. At this point, it is worth remembering that according to Mn L-edge XAS studies,[18] three Mn oxidation states, Mn^{2+}, Mn^{3+} and Mn^{4+}, coexist in calcium isostructural compounds. A similar situation can be expected for the Sr brownmillerites, so a complementary XANES study is required. Figure 3 shows the normalized Mn K-edge XANES spectra at room temperature of samples $La_{0.5}Sr_{0.5}MnO_{2.5}$ and $LaMnO_{2.75}$. Figure 3a shows a comparison of both spectra, because $LaMnO_{2.75}$ is taken as a reference with known 50% Mn^{2+} and 50% Mn^{3+} contents.[15,22] The corresponding Mn^{2+} and Mn^{3+} jumps needed to fit the $LaMnO_{2.75}$ absorption edge are also depicted. It is clear that the $La_{0.5}Sr_{0.5}MnO_{2.5}$ spectrum shows a higher contribution of Mn^{2+} jump, as can be observed by the high absorption in the 6540–6547 eV range.

To obtain the relative content of each Mn ion in the $La_{0.5}Sr_{0.5}MnO_{2.5}$ sample, the XANES spectrum was fitted by adding the separated contribution from each current ion in the sample. First, the fit of the $LaMnO_{2.75}$ reference (with known 50% Mn^{2+} and 50% Mn^{3+} contents)[15,22] experimental spectrum was checked. One arctangent function was used to account for each Mn oxidation state and an additional Gaussian function to reproduce the transition to the

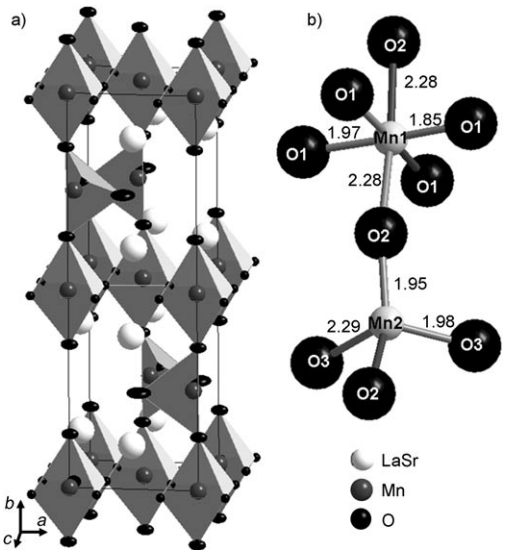

Figure 2. a) Schematic representation of the brownmillerite structure. The ellipsoids of the anisotropic thermal factors corresponding to O1 and O2 atoms are shown. b) Mn–O distances [Å] corresponding to $La_{0.5}Sr_{0.5}MnO_{2.5}$ at room temperature.

Table 2. Some selected interatomic distances [Å] in $La_{0.5}Sr_{0.5}MnO_{2.5}$ and $Nd_{0.5}Sr_{0.5}MnO_{2.5}$ at 300 and 5 K.

	$La_{0.5}Sr_{0.5}MnO_{2.5}$		$Nd_{0.5}Sr_{0.5}MnO_{2.5}$	
T [K]	300	5	300	5
Mn1–O1	1.972(17)×2	1.95(3)×2	1.902(17)×2	1.91(2)×2
Mn1–O1	1.850(17)×2	1.86(3)×2	1.895(17)×2	1.88(2)×2
Mn1–O2	2.286(3)×2	2.283(4)×2	2.254(2)×2	2.248(4)×2
Mn2–O2	1.951(6)×2	1.950(8)×2	1.935(5)×2	1.929(6)×2
Mn2–O3	1.98(3)	1.98(5)	2.12(3)	2.12(4)
Mn2–O3	2.29(2)	2.25(3)	2.251(16)	2.204(16)
Mn1-O1-Mn1	176.8(7)	175.1(13)	177.764(8)	177.5(1)
Mn2-O3-Mn2	110.9(1)	108.3(7)	105.2(2) 1	106.1(2)
Mn1-O2-Mn2	165.4(2)	164.4(3)	154.8(6)	155.2(5)

Table 3. BVS values calculated for manganese in $La_{0.5}Sr_{0.5}MnO_{2.5}$ and $Nd_{0.5}Sr_{0.5}MnO_{2.5}$ at 300 K.

Site geometry	$La_{0.5}Sr_{0.5}MnO_{2.5}$	$Nd_{0.5}Sr_{0.5}MnO_{2.5}$
octahedral Mn1	3.11	3.19
tetrahedral Mn2	1.98	1.90

4p states. A similar analysis has been carried out for $CaCu_3Mn_4O_{12}$ derivative compounds.[23] Within this fit analysis, the concentration of each Mn ion is related to its relative jump obtained from its corresponding arctangent function. The fit of the $LaMnO_{2.75}$ spectrum, with 50% Mn^{2+} and 50% Mn^{3+}, nicely reproduces the experimental data (Figure 3b).

Taking into account that the Mn^{2+} content should be higher in $La_{0.5}Sr_{0.5}MnO_{2.5}$ than $LaMnO_{2.75}$ (as seen in Figure 3a), and knowing that the average Mn oxidation state[13] in $La_{0.5}Sr_{0.5}MnO_{2.5}$ is also +2.5, we performed a fit of the Mn absorption K-edge by increasing (with respect to the reference 50%) the Mn^{2+} content and, simultaneously,

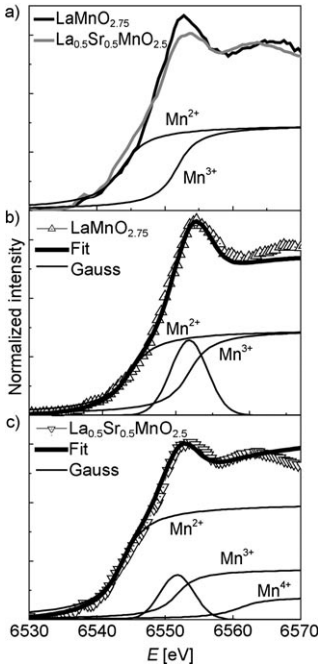

Figure 3. a) Experimental Mn K-edge XANES spectra of $LaMnO_{2.75}$ and $La_{0.5}Sr_{0.5}MnO_{2.5}$ at room temperature. b) Fit of the $LaMnO_{2.75}$ XANES spectrum with 50% Mn^{2+} and 50% Mn^{3+}. c) Fit of the $La_{0.5}Sr_{0.5}MnO_{2.5}$ XANES spectrum with 63% Mn^{2+}, 25% Mn^{3+} and 12% Mn^{4+}.

adding a Mn^{4+} content (equal to the Mn^{2+} increase) to preserve a constant oxidation state. It should be noted that this analysis is very accurate in the determination of the species contributing at the low-energy region of the edge spectra. In this way, the existence of Mn^{4+} is verified by a precise determination of Mn^{2+} content with the condition of +2.5 for the average Mn oxidation state. On the other hand, this kind of analysis is focused only on the determination of the oxidation states existing in the sample, in which only the jump edge is involved. For these reasons, the XANES oscillations (appearing from 6560 eV) cannot be reproduced by this analysis. Note that XANES oscillations are due to the scattering of photoelectrons from all lattice neighbours and, to simulate them, a multiple scattering analysis should be performed.

The spectrum of sample $La_{0.5}Sr_{0.5}MnO_{2.5}$ was subsequently simulated by using the function parameters obtained for Mn^{2+} and Mn^{3+} ($E_0(Mn^{2+})=6543.7$ eV and $E_0(Mn^{3+})=6551.8$ eV) as well as the Gaussian function, and including an additional Mn^{4+} contribution at $E_0=6561$ eV. The uncertainty in the obtained values was estimated by considering the goodness of the fit for different Mn ion fractions. As shown in Figure 3c, the fit confirms the coexistence of Mn in the three oxidation states with the following concentrations: 63±1% of Mn^{2+}, 25±3% of Mn^{3+} and 12±3% of Mn^{4+}. It is worth stressing that the presence of the obtained content of Mn^{3+} is absolutely mandatory to fit the $La_{0.5}Sr_{0.5}MnO_{2.5}$ spectrum. Actually, if no Mn^{3+} was present, the composition should be Mn^{4+} (25%)–Mn^{2+} (75%), which would lead to a very different threshold profile giving

an absorption overestimation in the 6540–6547 eV range and the opposite in the 6547–6555 eV one. These results are similar to those obtained by the analysis of Mn L-edge XAS quantification for the calcium isostructural brownmillerite ($La_{0.5}Ca_{0.5}MnO_{2.5}$).[18] BVS calculations together with XANES analysis allow confirmation that the octahedral layers would be occupied by 25% Mn^{4+}, 50% Mn^{3+} and 25% Mn^{2+}, whereas the tetrahedral one would be fully occupied by Mn^{2+}. The existence of Mn^{2+} and Mn^{3+} with a Jahn–Teller effect is in agreement with the presence of elongated octahedral layers.

Due to the system complexity, that is, three oxidation states for Mn distributed at the tetrahedral (Mn^{2+}) and octahedral positions (Mn^{2+}, Mn^{3+} and Mn^{4+}), the evolution of the diffraction pattern as a function of the temperature was followed (Figure 4). A similar behaviour is observed for the three samples. For this reason, only the data corresponding to $La_{0.5}Sr_{0.5}MnO_{2.5}$ are represented. Compared with the room-temperature observations, additional reflections, below 140 K for $La_{0.5}Sr_{0.5}MnO_{2.5}$, 130 K for $La_{0.5}Ca_{0.5}MnO_{2.5}$ and 120 K for $Nd_{0.5}Sr_{0.5}MnO_{2.5}$, appear. Their intensity gradually increases as the temperature decreases until a maximum value at around 5 K is reached. This behaviour indicates AFM ordering of Mn magnetic moments that start developing below the T_N, as indicated above.

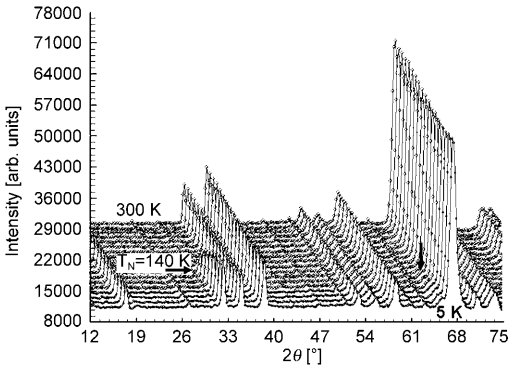

Figure 4. Thermal evolution of the ND pattern of $La_{0.5}Sr_{0.5}MnO_{2.5}$.

To deal with the magnetic structure of these brownmillerites, the refinement of the high-resolution diffraction data collected at 5 K was carried out. These data are also well described by the *Ibm*2 space group discussed above. The extra contributions to the diffraction patterns, which correspond to magnetic Bragg peaks, were analysed by using a magnetic unit cell with the same dimensions as the structural one with the propagation vector $k=(010)$. The calculated and experimental patterns corresponding to $La_{0.5}Sr_{0.5}MnO_{2.5}$ are shown in Figure 5. The results of the refinement of the best fit are summarized in Table 1 and the distances are collected in Table 2. The magnetic structure refinement for these compounds shows that the magnetic moments are aligned along the *b* axis of the unit cell (Figure 6). The magnetic moments of adjacent Mn atoms are antiferromagnetically coupled, not only in the Mn–O layers but also between them. Thus,

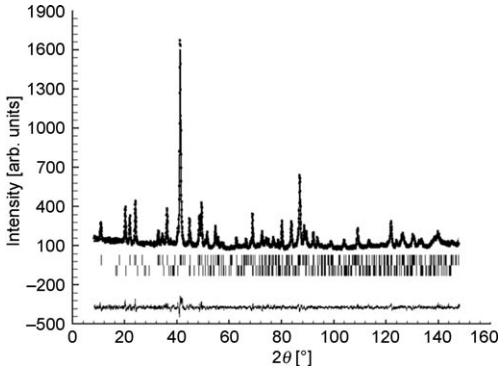

Figure 5. Observed, calculated and difference ND patterns corresponding to $La_{0.5}Sr_{0.5}MnO_{2.5}$ at 5 K.

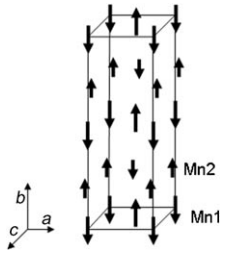

Figure 6. G-type AFM structure of $La_{0.5}Sr_{0.5}MnO_{2.5}$, $La_{0.5}Sr_{0.5}MnO_{2.5}$ and $Nd_{0.5}Sr_{0.5}MnO_{2.5}$ brownmillerites.

the magnetic moments of all Mn atoms are antiferromagnetically oriented relatively to the six nearest-neighbouring Mn atoms adopting a G-type AFM structure, according to the notations of the magnetic structures accepted for the 3D perovskite manganese oxides.[24] Similar strong G-type AFM coupling is reported for several other brownmillerite phases, such as $Ca_2Fe_2O_5$[25] and $Sr_2Co_{1.7}Ga_{0.3}O_5$,[19] with the moments parallel to the [001] direction or, for example, in $La_2Co_2O_5$[26] with the moments oriented parallel to [101]. The saturated magnetic moments of Mn1 and Mn2 are $\approx$2.6 and $\approx$1.6 μ_B (see Table 1 and Figure 7), respectively, for the three samples at 5 K.

We also followed the thermal evolution of the ND pattern, in the high-flux powder diffractometer, to establish the temperature dependence of the magnetic behaviour. The AFM ordering, described above, and its orientation is kept

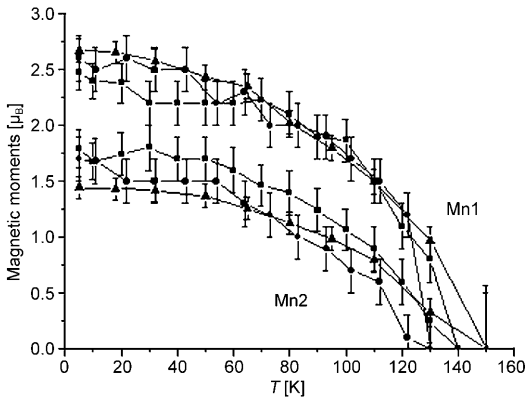

Figure 7. Magnetic moments for Mn cations as a function of temperature for $La_{0.5}Ca_{0.5}MnO_{2.5}$ (■), $La_{0.5}Sr_{0.5}MnO_{2.5}$ (▲) and $Nd_{0.5}Sr_{0.5}MnO_{2.5}$ (●) brownmillerites.

down to 5 K. The thermal variation of the ordered magnetic moments for Mn1 and Mn2 obtained from the refinement are shown in Figure 7. The fact that three brownmillerites exhibit the same magnetic moments in each layer is in perfect agreement with the same Mn composition detected by XANES. It is worth noting that, although Nd is a magnetic cation, it does not contribute to the total magnetization value because this cationic sub-lattice does not present magnetic order.

The magnetic characterization by means of ND reveals that $La_{0.5}Ca_{0.5}MnO_{2.5}$, $Nd_{0.5}Sr_{0.5}MnO_{2.5}$ and $La_{0.5}Sr_{0.5}MnO_{2.5}$ exhibit 3D ordering, which comprises a G-type AFM structure with T_N of 140 K for $La_{0.5}Sr_{0.5}MnO_{2.5}$, 130 K for $La_{0.5}Ca_{0.5}MnO_{2.5}$ and 120 K for $Nd_{0.5}Sr_{0.5}MnO_{2.5}$. This result is in agreement with previous magnetometry measurements.[13,14] However, differences are found for $La_{0.5}Sr_{0.5}MnO_{2.5}$ since FM interactions have been detected by magnetization measurements. Actually, there are very few examples of brownmillerite-related compounds with FM interactions and in most cases they comprise an A_2MBO_5 composition, M being a magnetic cation, such as Mn or Co, and B a non-magnetic cation.[11] In any case, the ND studies only reveal, again, AFM ordering, whereas additional FM behaviour is detected by magnetization measurements. This is the situation for Ca_2MnAlO_5 and Sr_2MnGaO_5,[9] SrCaMnGaO$_5$,[10] and even $Ca_2Fe_2O_5$,[25,27] with only Fe at the B sublattice. This fact would be related to the short range of the FM character, which provides a signal too weak to be detected in powder ND experiments. In this sense, it is mandatory to have a complementary study of ND and magnetometry measurements.

The origin of the unusual short-range-order FM in this structure has been tackled by other authors in different ways. For example, in $Ca_2Fe_2O_5$ material this double magnetic behaviour[27] is described on the basis of an AFM structure with spin canting. In the $La_{0.5}Sr_{0.5}MnO_{2.5}$ case, this situation is ruled out because the evolution of the FM and AFM contributions with the temperature is different. If the FM contribution were associated to the AFM structure, the FM behaviour would only be present in the temperature range associated to AFM order. However, the FM contribution in $La_{0.5}Sr_{0.5}MnO_{2.5}$ is kept at temperatures higher than T_N. On the other hand, in the $Sr_2MnGaO_{5+\delta}$ compound, the situation is different due to the presence of an oxygen excess.[7] Sr_2MnGaO_5 has a G-type AFM structure but the appearance of extra oxygen atoms in the Ga layers implies, as detected by ND, the appearance of small domains with G-type structure embedded into a matrix with C-type structure.

Finally, we propose that the FM interactions in $La_{0.5}Sr_{0.5}MnO_{2.5}$ would be related to the double exchange mechanism Mn^{3+}-O-Mn^{4+} in the octahedral layers.[13] This description contrasts with the absence of FM interactions in $La_{0.5}Ca_{0.5}MnO_{2.5}$ and $Nd_{0.5}Sr_{0.5}MnO_{2.5}$ even when Mn^{3+} and Mn^{4+} are also present. At this point it is worth remembering that FM interactions are present in the starting $La_{0.5}Sr_{0.5}MnO_3$ perovskite but not in $La_{0.5}Ca_{0.5}MnO_3$ and $Nd_{0.5}Sr_{0.5}MnO_3$; as a consequence, the optimal structural conditions, that is, Mn-O-Mn angles of around 180°, are only fulfilled by the La/Sr compound. In this sense, FM interactions in $La_{0.5}Sr_{0.5}MnO_{2.5}$ could be related to the presence of small clusters in the octahedral layers that kept the structural characteristics of the parent material. As a consequence of the short-range character of these clusters, the FM signal cannot be detected by ND experiments.

On the other hand, interesting information related to spin configuration on the three brownmillerites can be obtained. The saturated magnetic moments of Mn (Figure 7) are quite different from those expected when taking into account the Mn^{4+}, Mn^{3+} and Mn^{2+} arrangement into the octahedral and Mn^{2+} into the tetrahedral layers with their normal spin configuration. Starting with the tetrahedral layer, it should be noticed that this layer is fully occupied by the Mn^{2+}, which is, as has been detected in most of the compounds, present in the high-spin (HS) configuration. The magnetic moment associated with this configuration is 5.91 μ_B, much higher than the experimental one of $\approx$1.6 μ_B. Actually, there is a huge difference between the experimental and expected values for the Mn^{2+} magnetic moment, which suggests that the spin configuration must be different. A low-spin (LS) configuration is more plausible, because the associated magnetic moment would be 1.73 μ_B. This unusual phenomenon can be explained on the basis of the presence of the large Mn^{2+} cation in the smaller site, the tetrahedral one, which, in accordance with the radius estimation in a compact packing, is half the size of the octahedral one. This situation must lead to a high internal pressure that influences not only the structural distortion of the tetrahedra, but also their spin configuration. In this sense, it is well known[28–34] that high pressure favours the LS state because the LS ionic radius is, generally, smaller than that corresponding to the HS state. Moreover, the induced HS-to-LS transition pressure has been reported in metal transition oxides and sulfurs.[34]

In our case, external mechanical pressure was not applied, but it should be noted that the stabilization of the $Ln_{05}Sr_{0.5}MnO_{2.5}$ (Ln = La, Nd) and $La_{05}Ca_{0.5}MnO_{2.5}$ compounds requires special reducing conditions, under a H_2/He atmosphere, which allows the topotactic reduction process. The topotactic nature of the process forces an ordered structural reduction leading to Mn^{2+}, as a consequence of the reduction, in a tetrahedral environment because of the topotaxia. The optimal radii ratio corresponding to a tetrahedral hole is approximately 0.6 Å, while the ionic radius of Mn^{2+} in the HS configuration is 0.66 Å. This fact justifies the distortion of the tetrahedra and the LS state for Mn^{2+}, to reduce the generated tension as a consequence of the internal pressure at the tetrahedral sites. On the other hand, the magnetic value obtained in the octahedral layers (2.65 μ_B) is in agreement with those found in the parent perovskites in the same octahedral environment: $La_{0.5}Ca_{0.5}MnO_3$[35] (2.4 μ_B), $La_{0.5}Sr_{0.5}MnO_3$[36] (2.6 μ_B) and $Nd_{0.5}Sr_{0.5}MnO_3$[37] (2.7 μ_B).

Conclusion

The topotactic reduction of the manganese perovskites leads to $La_{0.5}Ca_{0.5}MnO_{2.5}$ and $Ln_{0.5}Sr_{0.5}MnO_{2.5}$ (Ln = La and Nd) brownmillerites that exhibit a G-type AFM structure. The ensemble of ND and XANES studies confirms the coexistence of Mn^{2+}, Mn^{3+} and Mn^{4+} as well as their arrangement at the tetrahedral (Mn^{2+}) and octahedral (Mn^{2+}, Mn^{3+}, Mn^{4+}) layers. It is worth reinforcing that Mn^{2+}, which is the biggest cation, in principle occupies the smaller sites, that is, the tetrahedral ones. This situation is linked to the magnetic moment attained for the tetrahedral layers and suggests the stabilization of Mn^{2+} in the LS configuration. FM interactions detected in $La_{0.5}Sr_{0.5}MnO_{2.5}$ by means of magnetization measurements, but not in the ND study, can be explained on the basis of small FM clusters with Mn^{3+}-O-Mn^{4+} 180° angles that persist on $La_{0.5}Sr_{0.5}MnO_{2.5}$ as a consequence of the topotactic nature of the reducing process.

Experimental Section

$La_{0.5}Ca_{0.5}MnO_{2.5}$, $La_{0.5}Sr_{0.5}MnO_{2.5}$ and $Nd_{0.5}Sr_{0.5}MnO_{2.5}$ were synthesized by controlled reduction of $La_{0.5}Ca_{0.5}MnO_3$, $La_{0.5}Sr_{0.5}MnO_3$ and $Nd_{0.5}Sr_{0.5}MnO_3$, respectively. To obtain enough mass to carry out a ND study, the samples were prepared in a Cahn D-101 electrobalance. Reduced samples (1.5 g) were obtained by heating the starting perovskite material at 630 °C under a continuous flux of 50 % H_2 and 50 % Ar at a rate of 0.1 °C min^{-1}. Once the desired weight loss had been attained, the sample was annealed at 630 °C under an Ar atmosphere for 48 h to facilitate a more homogeneous distribution of the anionic vacancies. Further details of topotactic reduction have been reported elsewhere.[12–14] Neutron powder diffraction data were collected at the Institut Laue-Langevin (ILL). The data were acquired on the high-resolution powder diffractometer D2B at 5 and 300 K, with neutrons of wavelength 1.594 Å. To follow the evolution of the magnetic structure with temperature, ND data were obtained on the high-flux powder diffractometer D1B at a wavelength of 2.52 Å. Diffraction data were analysed by the Rietveld method[38] using the Fullprof program.[39] XAS experiments were carried out at the BM25 beamline (SpLine) of the European Synchrotron Radiation Facility (ESRF), with a storage-ring energy of 6 GeV and an average current of 200 mA. A Si(111) double-crystal pseudo-channel-cut monochromator was used for energy selection and the sample was vertically shifted while the spectrum was collected. The incident beam was monitored by means of an ion chamber filled with a mixture of N_2 and He. The monochromator was detuned up to 30 % for those energy ranges to reject components of higher harmonics. Measurements were developed in fluorescence mode due to the high absorption from the sample. Spectra were obtained at room temperature using a geometry in which the detector forms an angle of 90° with respect to the incoming beam. Several spectra were collected to improve the statistics and give a good signal-to-noise ratio. $LaMnO_{2.75}$, obtained by topotactic reduction of $LaMnO_{3.00}$,[15,22] was used as a reference for XANES.

Acknowledgements

Financial support from Ministerio de Educación y Ciencia (Spain) through the research project MAT2007-61954 is acknowledged. Fruitful discussions with Dr. M. T. Fernandez-Diaz (ILL, Grenoble, France) are also acknowledged.

[1] Y. Tsujimoto, C. Tassel, N. Hayashi, T. Watanabe, H. Kageyama, K. Yoshimura, M. Takano, M. Ceretti, C. Ritter, W. Paulus, *Nature* **2007**, *450*, 1062–1065.
[2] J. Köhler, *Angew. Chem.* **2008**, *120*, 4544–4546; *Angew. Chem. Int. Ed.* **2008**, *47*, 4470–4472.
[3] J. C. Grenier, M. Pouchard, P. Hagenmuller, *Mater. Res. Bull.* **1976**, *11*, 1219–1226.
[4] W. C. Hansen, L. T. Brownmiller, R. H. Bogue, *J. Am. Chem. Soc.* **1928**, *50*, 396–414.
[5] M. Von Harden, H. Müller-Buschbaum, *Z. Anorg. Allg. Chem.* **1980**, *464*, 169–175.
[6] W. T. A. Harrison, T. H. Lee, Y. L. Yang, D. P. Scarfe, L. M. Liu, A. Jacobson, *Mater. Res. Bull.* **1995**, *30*, 621–630.
[7] V. Y. Pomjakushin, A. M. Balagurov, T. V. Elzhov, D. V. Sheptyakov, P. Fischer, D. I. Khomskii, V. Y. Yushankhai, A. V. Abakumov, M. G. Rozova, E. V. Antipov, M. V. Lobanov, S. J. L. Billinge, *Phys. Rev. B* **2002**, *66*, 184412.
[8] T. Siegrist, S. Sunshine, D. W. Murphy, R. J. Cava, S. M. Zahurak, *Phys. Rev. B* **1987**, *35*, 7137–7139.
[9] J. Wright, H. M. Palmer, P. A. Anderson, C. Greaves, *J. Mater. Chem.* **2002**, *12*, 978–982.
[10] P. D. Battle, A. M. Bell, S. J. Blundell, A. I. Coldea, D. J. Gallon, F. L. Pratt, M. J. Rosseinsky, C. A. Steer, *J. Solid State Chem.* **2002**, *167*, 188–195.
[11] A. M. Abakumov, M. G. Rozova, E. V. Antipov, *Russ. Chem. Rev.* **2004**, *73*, 847–860.
[12] J. M. González-Calbet, E. Herrero, N. Rangavittal, J. M. Alonso, J. L. Martínez, M. Vallet-Regí, *J. Solid State Chem.* **1999**, *148*, 158–168.
[13] R. Cortés-Gil, M. L. Ruiz-González, J. M. Alonso, M. Vallet-Regí, A. Hernando, J. M. González-Calbet, *Chem. Eur. J.* **2007**, *13*, 4246–4252.
[14] L. Ruiz-González, R. Cortés-Gil, J. M. Alonso, J. M. González-Calbet, M. Vallet-Regí, *Open Inorg. Chem. J.* **2007**, *1*, 37–46.
[15] M. L. Ruiz-González, R. Cortés-Gil, J. M. Alonso, A. Hernando, M. Vallet-Regí, J. M. González-Calbet, *Chem. Mater.* **2006**, *18*, 5756–5763.
[16] P. S. Casey, D. Barker, M. A. J. Hayward, *J. Solid State Chem.* **2006**, *179*, 1375–1382.
[17] Y. Tokura in *Advances in Condensed Matter Science, Vol. 2* (Eds.: Y. Tokura), Gordon & Breach Science Publishers, Amsterdam, **2000**, pp. 2–6.
[18] J. M. Alonso, R. Cortés-Gil, L. Ruiz-González, J. M. González-Calbet, A. Hernando, M. Vallet-Regí, M. E. Dávila, M. C. Asensio, *Eur. J. Inorg. Chem.* **2007**, *21*, 3350–3355.
[19] F. Lindberg, S. Y. Istomin, P. Berastegui, G. Svensson, S. M. Kazakov, E. V. Antipov, *J. Solid State Chem.* **2003**, *173*, 395–406.
[20] P. Berastegui, S. Hull, F. J. García-García, S. G. Erikson, *J. Solid State Chem.* **2002**, *164*, 119–130.
[21] C. Greaves, A. J. Jacobson, B. C. Tofield, B. E. F. Fender, *Acta Crystallogr. Sect. B* **1975**, *31*, 641–646.
[22] F. Abbattista, M. L. Borlera, *Ceram. Int.* **1981**, *7*, 137–141.
[23] J. Sánchez-Benítez, C. Prieto, A. de Andrés, J. A. Alonso, M. J. Martínez-Lope, M. T. Casais, *Phys. Rev. B* **2004**, *70*, 024419.
[24] E. O. Wollan, W. C. Koehler, *Phys. Rev.* **1955**, *100*, 545–563.
[25] S. Geller, R. W. Grant, U. Gonser, M. Wiedresich, G. P. Espinosa, *Phys. Lett.* **1966**, *20*, 115.
[26] O. H. Hasnteen, H. Fjellvag, B. C. Hauback, *J. Solid State Chem.* **1998**, *141*, 411–417.
[27] P. Marchukov, R. Geick, C. Brotzeller, W. Treutmann, E. G. Rudashevsky, A. M. Balbashov, *Phys. Rev. B* **1993**, *48*, 13538–13546.
[28] R. E. Cohen, I. Mazin, D. G. Isaak, *Science* **1997**, *275*, 654–657.
[29] M. P. Pasternak, R. D. Taylor, R. Jeanloz, X. Li, J. H. Nguyen, C. A. McCammon, *Phys. Rev. Lett.* **1997**, *79*, 5046–5079.
[30] I. Troyan, A. G. Gavrilyuk, V. A. Sarkisyan, I. S. Lyubutin, R. Ruffer, O. Leopold, A. Barla, B. Doyle, A. I. Chumakov, *JETP Lett.* **2001**, *74*, 26–29.

[31] W. M. Xu, O. Naaman, G. K. Rozenberg, M. P. Pasternak, R. D. Taylor, *Phys. Rev. B* **2001**, *64*, 094411.
[32] J. Badro, G. Fiquet, F. Guyot, J.-P. Rueff, V. V. Struzhkin, G. Vankó, G. Monaco, *Science* **2003**, *300*, 789–791.
[33] A. G. Gavriliuk, I. A. Troyan, R. Boehler, M. I. Eremets, I. S. Lyubutin, N. R. Serebryanaya, *JETP Lett.* **2003**, *77*, 747–752.
[34] K. Persson, G. Ceder, G. Morgan, *Phys. Rev. B* **2006**, *73*, 115201.
[35] Q. Huang, J. W. Lynn, R. W. Erwin, A. Santoro, D. C. Dender, V. N. Smolyaninova, K. Ghosh, R. L. Greene, *Phys. Rev. B* **2000**, 61, 8895–8905.
[36] O. Chmaissem, B. Dabrowski, S. Kolesnik, J. Mais, J. D. Jorgensen, S. Short, *Phys. Rev. B* **2003**, *67*, 094431.
[37] R. Kajimoto, H. Yoshizawa, H. Kawano, H. Kuwahara, Y. Tokura, K. Ohoyama, M. Ohashi, *Phys. Rev. B* **1999**, *60*, 9506–9517.
[38] H. M. Rietveld, *J. Appl. Crystallogr.* **1969**, *2*, 65–71.
[39] J. Rodríguez-Carvajal, *Physica B* **1993**, *192*, 55.

Received: April 15, 2008
Published online: August 7, 2008

